EUROPEAN FUSION DEVELOPMENT AGREEMENT

EFDA–JET–PR(04)61

T. Tala, L. Laborde, D. Mazon, D. Moreau, G. Corrigan, F. Crisanti,
X. Garbet, D. Heading, E. Joffrin, X. Litaudon, V. Parail, A. Salmi
and JET EFDA contributors

# Fully Predictive Simulations of Current and Temperature Profile Control in JET Advanced Tokamak Plasmas and Comparison with Experiments

# Fully Predictive Simulations of Current and Temperature Profile Control in JET Advanced Tokamak Plasmas and Comparison with Experiments

T. Tala[1], L. Laborde[2], D. Mazon[2], D. Moreau[2, 3], G. Corrigan[4], F. Crisanti[5], X. Garbet[2], D. Heading[4], E. Joffrin[2], X. Litaudon[2], V. Parail[4], A. Salmi[6] and JET EFDA contributors*

*[1]Association EURATOM-Tekes, VTT Processes, P.O. Box 1608, FIN-02044 VTT, Finland*
*[2]Association EURATOM-CEA, CEA/DSM/DRFC Cadarache, St Paul-Lez-Durance, France*
*[3]EFDA-JET, Culham Science Centre, Abingdon, Oxon. OX14 3DB, UK*
*[4]EURATOM/UKAEA Fusion Association, Culham Science Centre, Oxon. OX14 3DB, UK*
*[5]Associazione EURATOM-ENEA sulla Fusione,Via Enrico Fermi 27, 00044 Frascati, Italy*
*[6]Association EURATOM-Tekes, Helsinki University of Technology, FIN-02015 TKK, Finland*
** See annex of J. Pamela et al, "Overview of Recent JET Results and Future Perspectives", Fusion Energy 2002 (Proc.19 th IAEA Fusion Energy Conference, Lyon (2002).*

Preprint of Paper to be submitted for publication in
Nuclear Fusion

**ABSTRACT**

For the first time fully predictive, time-dependent transport simulations with a non-linear plasma model (Bohm/GyroBohm transport model) have been used in closed-loop simulations to control the $q$-profile and the strength and location of the ITB. Five transport equations ($T_e$, $T_i$, $q$, $n_e$, $v_\Phi$) are solved, and the power levels of LHCD, NBI and ICRH are calculated in a feedback loop determined by the feedback controller matrix. The real-time control technique and algorithms used in the transport simulations are identical to those implemented and used in JET experiments. The closed-loop simulations with real-time control demonstrate that varieties of $q$-profiles and pressure profiles in the ITB can be achieved and controlled simultaneously. The simulations also showed that with the same real-time control technique as used in JET experiments, it is possible to sustain the $q$-profiles and pressure profiles close to their set-point profiles for longer than the current diffusion time. The importance of being able to handle the multiple time scales to control the location and strength of the ITB is demonstrated. Several future improvements and perspectives of the real-time control scheme are presented.

## 1. INTRODUCTION

The perspective of ITER and the need to optimise the tokamak concept for the design of an economical fusion power plant have motivated extensive international research on plasma transport and confinement in toroidal devices. These investigations have led to plasma regimes with improved confinement with respect to the one predicted by typical tokamak scaling laws, and to the concept of "advanced tokamak" operation scenarios [1]. In a large number of machines, experiments have demonstrated the existence of such regimes allowing access to a high confinement state with improved MHD stability and leading to a strong increase of the plasma performance quantified by the normalized energy confinement time, $H$-factor, and plasma pressure, $\beta_N$. In such conditions a dominant fraction of the plasma current is self-generated by the neoclassical bootstrap mechanism, which alleviates the requirement on the externally driven non-inductive current for steady state operation. This is helped by the generation of a so-called 'Internal Transport Barrier' (ITB) [2], a region where the plasma turbulence is almost suppressed, and that can lead to a sustainable bifurcated plasma equilibrium. Many recent studies have shown the key influence, of the safety factor radial profile, $q$(r) for the triggering of ITB's [3]. The magnetic shear, $s=(r/q)(\mathrm{d}q/\mathrm{d}r)$, and/or the location of the magnetic flux surfaces where $q$ is rational have been shown to be important for the emergence of ITBs [3-6], thus giving a strong motivation to control ITBs in real-time.

An important experimental programme is in progress on JET to investigate plasma control schemes which could eventually enable ITER to sustain steady-state burning plasmas in an "advanced tokamak" operation scenario. The triggering and subsequent controllability of ITBs are major issues for fulfilling this goal, and their study is therefore an essential part of this programme. Uncontrolled ITBs are generally not stationary, as often observed on JET, and the coupled evolution of the plasma parameter profiles in high performance non-inductive discharges often leads to the premature loss of the good confinement ITB regime, or alternatively to an overpeaking of the pressure profile,

with major MHD events, sudden barrier collapse and/or abnormal plasma termination. Recently, a multi-variable model-based technique was developed [7-11] for the simultaneous control of the current, temperature and/or pressure profiles in JET ITB discharges, using Lower Hybrid Current Drive (LHCD) together with NBI and ICRH. The Real-Time Control (RTC) scheme relies on the experimental identification, and on a Truncated Singular Value Decomposition (TSVD), of a linearized integral model operator. The justification for using linear response models to design controllers for non-linear systems is that, if it works, the system should not depart largely from the requested equilibrium since the controller is to provide stability around it. Therefore, a control matrix defined through linearization can often provide an acceptable solution. The proposed technique retains the intrinsic couplings between the plasma parameter profiles, as well as their distributed nature by using an appropriate set of trial basis functions. The related algorithms have been implemented in the JET control system, allowing the use of three actuators that are the power levels of NBI, ICRH and LHCD systems. The identical algorithms to those used in the experiments have been also implemented in the JETTO transport code [12,13]. This paper reviews primarily the progress achieved in fully predictive transport modelling of ITB plasmas when applying the real-time control algorithms in the transport simulations to control the $q$-profile and the strength and location of the ITB (electron temperature and electron temperature gradient profile).

Although plasma transport, in particular that of the ITB, cannot be described perfectly with present transport codes and models, there are several reasons why the real-time control techniques have been implemented in transport codes in parallel with the experiments. One reason is that high power RTC experiments on JET are limited to about 10s due to restrictions on the NBI power system. This is less or at most of the order of the resistive current diffusion time on JET and therefore, extending the simulations to pulse lengths well beyond this time is useful to further assess the validity of the control scheme for steady state operation. Another reason is that the identification of linear state-space models is difficult from the experimental data due to unsatisfactory data quality from the measurements and data pollution by the MHD events such as ELMs and NTMs whereas the transport simulation data is free from them and can be used for developing the required skills for an optimum identification scheme. Thirdly, the transport simulations can be used in the determination of the control matrix, in view of using it also in the RTC experiments. And lastly, the transport simulations with RTC can be used to test and validate different versions of the control algorithms, with increasing degrees of completeness, before implementing them in the experimental control systems.

The paper is organised as follows. The description on how to perform transport simulations with RTC in the JETTO transport code is illustrated in section 2. In addition, the motivations for using fully predictive transport simulations and the Bohm/GyroBohm transport model with the empirical ITB threshold condition [4] are given. Section 3 is devoted to the transport modelling with controlling only one plasma profile in real-time. This is either the $q$-profile or the electron temperature profile in the ITB. The results from the transport simulations with the simultaneous real-time control of $q$ and ITB are presented in section 4. In section 5, the experimental results on JET ITB plasmas are

illustrated when the same RTC technique as used in the simulations, is applied. In addition, the experimental results are compared with those from the transport simulations. The conclusions are discussed and the future perspectives are drawn in section 6.

## 2. USE OF REAL-TIME CONTROL TECHNIQUE IN THE JETTO TRANSPORT CODE

JETTO is a one and a half dimensional integrated transport modelling code solving the time-dependent transport equations averaged over the magnetic flux surfaces [12]. There are several options for example for the equilibrium calculation, handling the heating and current drive, boundary conditions etc. in the code. Based on the past experience on ITB modelling, it has turned out to be crucial to make fully predictive transport simulations, in order to obtain as self-consistent and reliable predictions as possible for the dynamics of the ITB [13,14]. The concept of 'full predictability' means that five transport equations are solved, i.e. ion and electron heat transport, particle transport, toroidal momentum transport and current diffusion. Thus, the simulations yield predictions for $T_i$, $T_e$, $n_e$, $v_{\Phi,}$ and $q$, respectively.

The semi-empirical Bohm/GyroBohm transport model with its empirical ITB threshold condition has been used in all the simulations performed in this work [4]. It has been found very recently to be the most satisfactory transport model to reproduce the time dynamics of the strength and location of ITB with the dependent simulations in a multi-tokamak ITB database [13]. However, the real-time control algorithms implemented in JETTO are fully modular and thus independent of the choice of the transport model. The typical prediction accuracy for the ITB dynamics in time-dependent transport simulations (lasting for several seconds) is illustrated in Fig. 1 for two JET ITB discharges when using the Bohm/GyroBohm [4,15] and Weiland transport models [16]. The prediction errors are typically less than 20% for the plasma profiles and about 10cm or less for the radial location of the ITB when using the Bohm/GyroBohm transport model. For the first-principle transport models, the prediction errors are larger. The left-hand side pulse (Pulse no: 46664) represents a case with a monotonic $q$-profile while the discharge on the right-hand side (Pulse no: 53521) is an example of a pulse with a reversed $q$-profile. It also represents one of the worst simulations in terms of prediction accuracy when using the Bohm/GyroBohm model in JET [13,14]. All the neo-classical quantities, such as the bootstrap current, electrical resistivity, poloidal rotation and neo-classical ion heat diffusivity are calculated inside JETTO by the NCLASS transport code [17].

In order to be able to control the coupled evolution of the pressure and current density profiles in ITB pulses, a multi-variable model-based technique has been developed and used in JET [7]. It relies on the determination of a linearized integral model operator identified from either power modulation experiments or fully predictive modulation simulations around a target steady-state. In this work, we present results when using the predictive simulations for the determination of the controller.

The model-based control technique applied to the design of a Multiple-Input-Multiple-Output (MIMO) controller is proposed for achieving steady state regimes in JET with a given $q$ and $\rho_{Te}^{*}$-profiles. $\rho_{Te}^{*}$ is defined as the ratio between the Larmor radius and the electron temperature gradient

length, and is used to characterise the strength and location of ITBs in JET. According to the empirical database analysis performed in JET, a criterion for the existence of an ITB can be written as follows [18]:

$$\rho^{*}_{Te}(x,t) \geq 0.014\,. \tag{1}$$

The model retains the distributed nature of the plasma parameter profiles to be controlled using an appropriate set of trial basis functions $a_i(x)$ and $b_j(x)$. The projection of $q$ onto a set of spline basis functions $a_i(x)$ and $\rho_{Te}^{*}$ onto a set of triangular basis functions $b_j(x)$ is performed in the Galerkin sense inside JETTO. It produces an acceptable approximation of those profiles [9]

$$q(x) = \sum_{i=1}^{5} Gq_i a_i(x) \qquad\qquad \rho^{*}_{Te}(x) = \sum_{j=1}^{3} G\rho^{*}_{Tej} b_j(x)\,, \tag{2}$$

where $Gq_i$ and $G\rho_{Tej}^{*}$ are called the Galerkin coefficients and are calculated in real time from the simulated profiles. The feedback control of the $q$ and $\rho_{Te}^{*}$ profiles have been restricted to the radial regions $0.2 \leq r/a \leq 0.8$ and at $0.4 \leq r/a \leq 0.6$, respectively (the ITB is typically expected and required in the latter region). The set-point values for $q$ and $\rho_{Te}^{*}$ are given as input parameters for JETTO at five and three radial points (called knots), respectively. However, the number of knots for $q$ and $\rho_{Te}^{*}$ is an input parameter in JETTO, but in the simulations presented in this paper we have restricted to the given values, as doing everything as similarly to the experiments as possible. These numbers also define the number of basis functions $a_i(x)$ and $b_j(x)$, as indicated by the summations in equations (2). The linearized Laplace response function around the target equilibrium can be written as follows:

$$G(s) = K(s)P(s)\,, \tag{3}$$

where $G(s)$ represents a matrix (8 x 1, i.e. number of knots in for $q$ and $\rho_{Te}^{*}$ used) of the Galerkin coefficients of $´q(x,s)$ and $´\rho_{Te}^{*}(x,s)$ profiles modifications when a modulation power $P(s)$ (3 x 1 matrix) is applied. The kernel $K(s)$ (8 x 3 matrix) in this work is identified from the fully predictive power modulation simulations using the JETTO transport code as described above. As the first step, however, only the steady state gain matrix $K(0)$ was used and it was deduced from simple step power changes in JETTO open-loop simulations.

After making a truncated singular value decomposition and using some matrix algebra, one can write the real-time controller transfer function $H(s)$ as follows [7,9]:

$$P(s) = H(s)G(s) = g_c\left[1 + {}^{1}\!\!\diagup\!\!{}_{\tau_i s}\right]K_{inv}G(s)\,, \tag{4}$$

where $g_c$ is the proportional gain, $g_c/\tau_i$ is the integral gain and $K_{inv}$ is a truncated (singular value decomposition) inverse matrix of $K(0)$ when taking into account the Galerkin scheme for $q$ and $\rho_{Te}^{*}$ as done in Ref. [7]. The schematic diagram on how the feedback control loop and the controller

transfer function $H$(s) work is illustrated in Fig. 2. $E$(s) is the error signal denoting the difference between the simulated and set-point $q$-profiles or $\rho_{\mathrm{Te}}^{*}$-profiles.

Now we can write equation (4) in time coordinate $t$ instead of the Laplace coordinate $s$, in order to see how the power levels of LHCD, NBI and ICRH are controlled in the closed-loop simulations with real-time control

$$\begin{bmatrix} P_{LHCD}(t) \\ P_{NBI}(t) \\ P_{ICRH}(t) \end{bmatrix} = [P_0] + g_c K_{inv} \left\{ (G_{ref} - G_{sim}(t)) + 1/\tau_i \int_{t_0} (G_{ref} - G_{sim}(t)) dt \right\}. \quad (5)$$

Here $P_0$ is the vector containing the power levels of LHCD, NBI and ICRH at $t_0$ (when the real-time control starts) and $G_{\mathrm{ref}}$ and $G_{\mathrm{sim}}$ represents Galerkin coefficients of the set-point and simulated profiles of $q$ and $\rho_{\mathrm{Te}}^{*}$ (at time $t$). This controller minimises the following integral (squared distance between the set-point and simulated profiles at time $t$):

$$dy^2 = dq^2 + \mu d\rho_{Te}^{*2} = \int_{0.2}^{0.8} (q(x) - q_{set}(x))^2 dx + \mu \int_{0.4}^{0.6} (\rho_{Te}^{*}(x) - \rho_{Te,set}^{*}(x))^2 dx, \quad (6)$$

where $^{o}$ is a tuning factor for the relative weight on RTC between the square distances of the set-point and simulated $q$-profiles and $\rho_{\mathrm{Te}}^{*}$-profiles, i.e. $dq^2$ versus $d\rho_{\mathrm{Te}}^{*2}$. The tuning factor is used in the determination of the feedback control matrix from the JETTO open-loop simulations. In all the simulations in this study where both $q$ and $\rho_{\mathrm{Te}}^{*}$ are controlled simultaneously, the value of $^{o}$ was set to 70000. In the case of the $q$-profile control only, we set $^{o}$=0.0 and in the case of the $\rho_{\mathrm{Te}}^{*}$-profile control only, we set $^{o}$ to be a very large number.

The power deposition and driven current density profiles of the three actuators in JETTO transport simulations are calculated with the following codes: FRTC [19] for LHCD, PENCIL [20] for NBI and PION [21] for ICRH. LHCD and NBI, which are rather sensitive to variations in plasma kinetic profiles, are calculated self-consistently inside JETTO whereas the ICRH power deposition profile is calculated with the PION code outside JETTO. The power levels of the three actuators in closed-loop simulations, i.e. when applying the RTC technique, are fully determined from the difference between the set-point (target) and simulated values of $q$ and $\rho_{\mathrm{Te}}^{*}$ multiplied by the feedback control matrix $K_{\mathrm{inv}}$ as shown in equation (5). A schematic illustration on how the open- and closed-loop transport simulations are performed with JETTO is presented in Fig. 3. All the simulations start typically around $t$=4s (indicated by the vertical dash-dotted line). The power step-ups in the open-loop simulations (such as the solid line) are made when the discharge is rather stationary, typically around $t$=15s and the steady-state response, i.e. the calculation of the feedback controller matrix, is taken at around $t$=30s (dashed vertical line). In the closed-loop simulations the real-time control starts typically at $t$=5.5s (dashed vertical line), and RTC can be applied as long as desired, typically for more than one resistive current diffusion time. The power levels vary in the closed-loop simulations (dashed curve), as requested by the controller according to equation (5). The whole procedure of carrying out the open-loop power step-up simulations, determination of the controller

matrix from the open-loop simulations and finally performing the closed-loop simulations with RTC is identical to that performed in JET experiments when applying the RTC technique.

## 3. REAL-TIME CONTROL OF THE *Q*-PROFILE OR THE ELECTRON TEMPERATURE PROFILE IN AN ITB

In this section, the simulation results when controlling only one plasma profile at a time, either the $q$-profile or the $\rho_{Te}^{*}$-profile (normalised electron temperature gradient in the ITB) are presented. In all the simulations, the magnetic field, the plasma current, $Z_{eff}$, the initial and boundary conditions and the power levels of LHCD, NBI and ICRH until the control starts are taken from JET Pulse no: 62527. The experimental results, including also this discharge, will be discussed briefly in section 5. The experimental discharge lasted only until $t$=9.2s. As a consequence, in the JETTO simulations lasting beyond $t$=9.2s, the magnetic field, the plasma current, the boundary conditions etc. are kept at the level of those at $t$=9.2s. The equilibrium is calculated with the ESCO equilibrium solver inside JETTO using the plasma boundaries calculated by EFIT [22].

The modelling results obtained in the closed-loop simulations when applying the real-time control only to the $q$-profile are illustrated in Figs. 4–7. Three simulations are compared, one closed-loop simulation with a reversed set-point $q$-profile (solid curves), one closed-loop simulation with a monotonic set-point $q$-profile (dashed curves) and a reference open-loop simulation with constant power levels (dotted curves).

Although the set-point $q$-profiles are reached with a good accuracy in both the reversed shear and monotonic $q$ cases, there are several issues in Figs. 4–7 worth commenting. Firstly, the time when the set-point $q$-profiles are achieved is rather long, of the order of 10s after the start of the control, thus being significantly longer than observed in the experiments. This is due to two facts. Firstly, the initial $q$-profile in the simulations when the control starts is further away from the set-point ones than in the experiments and secondly, because of being far from the set-point $q$-profiles, smaller proportional ($g_c$) and integral gains ($g_c/\tau_i$) than used in the experiments must have been adopted in the simulations. The further the set-point profiles are from the simulated starting values, the smaller values for the gains are needed to ensure the stability of the controller. The reason for choosing such extreme set-point $q$-profiles is to explore on how far the initial $q$-profiles, when using the present RTC algorithms, still converge to the set-point ones. The second peculiar feature in the simulation results is that in the case of the reversed set-point $q$-profile, the closed-loop simulation converges towards the set-point $q$-profile in a somewhat unexpected way, i.e. turning off the NBI and ICRH powers and increasing the LHCD power above 6MW. On the other hand, in the case of the monotonic set-point $q$-profile, the closed-loop simulation first decreases all the three powers in order to get rid of the ITB. This enables it to gradually get rid of the large off-axis bootstrap current due to the ITB which would otherwise prevent the current from peaking on axis and thus, $q$ from becoming gradually monotonic.

As was shown in Figs. 4–7, a reversed $q$-profile does not necessarily guarantee a good fusion performance if it has been achieved by switching-off the NBI and ICRH powers. Therefore, the

real-time control of the ITB in addition to the RTC of $q$ is also needed. As the simulations are carried out identically to the JET RTC experiments, $\rho_{Te}^*$ is the quantity to be used to control the electron temperature gradient in ITBs in real time. Similar time traces and profiles as shown in Figs. 4–7, but with the $\rho_{Te}^*$ control only are illustrated in Figs. 8–11. Three simulations are compared, one closed-loop simulation with a strong ITB as the set-point $\rho_{Te}^*$-profile (solid curves), one closed-loop simulation with a weak ITB as the set-point $\rho_{Te}^*$-profile (dashed curves) and a reference open-loop simulation with constant power levels (dotted curves). The reference open-loop simulation is the same as shown in Figs. 4–7.

As with RTC of the $q$-profile only, the $\rho_{Te}^*$-profiles reach their set-point profiles in the closed-loop simulations, both in the strong and weak ITB set-point cases. However, two special issues originating from the simulation results presented in Figs. 8–11 must be addressed. Firstly, in the closed-loop simulation with the 'strong ITB' as the set-point $\rho_{Te}^*$-profile, the simulation approaches the requested $\rho_{Te}^*$-profile, but only in the electron heat transport channel, as shown in Figs 11. In fact, the ion temperature and the ion temperature gradient are the smallest in the simulation with the strong ITB as the set-point $\rho_{Te}^*$-profile. This is justified by the RTC controller because $\rho_{Te}^*$ measures and controls the electron temperature gradient, rather than the ion one. However, from the fusion performance point of view, the ITB on the ion heat transport channel is more desirable. This indicates that the control of $\rho_{Ti}^*$ (ion Larmor radius divided by the ion temperature gradient length) could be as relevant or even a more relevant quantity to be real-time controlled. However, since the time and spatial resolutions of the ion temperature measurements, in particular in real-time, have been much poorer on JET than the electron temperature measurements, the experiments so far have focused on the control of electron ITB's through $\rho_{Te}^*$.

As the second special issue, the closed-loop simulations in Figs. 8–11 demonstrate the existence of a double time scale even in the case when controlling $\rho_{Te}^*$-profiles only. Initially before the control starts and still at $t$=10s, the ITB is located at ¡≈$r/a$≈0.35 while the set-point $\rho_{Te}^*$ requests that it should be at $r/a$≈0.5. However, although the temperature profiles can be changed in principle on the energy confinement time scale, moving the ITB 15cm outwards, i.e. changing the position of the peak in the $\rho_{Te}^*$-profile, takes a much longer time. This is due to the fact that the location of the ITB (and the ITB dynamics in general) is strongly coupled with the $q$-profile and magnetic shear evolution. As a consequence, moving the footpoint of the ITB 15cm outwards may actually take a time of the order of the resistive current diffusion time, to allow significant changes in the $q$-profile to occur. Therefore, $\rho_{Te}^*$-profile control is governed by physical phenomena occurring on two very different time scales, i.e. the energy confinement and current diffusion time scales. These simulations therefore support the design of a double time scale real-time controller for a successful ITB control in discharges whose duration will be of the order of the resistive current diffusion time.

In order to be able to have a scenario with a reversed $q$-profile and a strong ITB (also on ions), a simultaneous real-time control of both the $q$-profile and $\rho_{Te}^*$-profile, and possibly and preferably also $\rho_{Ti}^*$-profile, is needed. These types of set-point profiles maximise simultaneously the high fusion performance and high non-inductive current fraction, giving perspective for steady-state

tokamak operation, and very importantly, with real-time control of the key plasma profiles. The simulation predictions with a combined real-time control of the $q$-profile and $\rho_{Te}^{*}$-profile on a time scale of several current diffusion times are presented in section 4.

## 4. SIMULTANEOUS REAL-TIME CONTROL OF THE *Q*-PROFILE AND THE ELECTRON TEMPERATURE PROFILE IN THE ITB

The choice for the set-point $q$-profiles and $\rho_{Te}^{*}$-profiles is more delicate in the case of the simultaneous control than with a single profile real-time control. There is only a limited family of [$q$, $\rho_{Te}^{*}$] profile pairs that are achievable, in particular if the power level limitations on JET are taken into account. Similarly to Figs. 4–7 and 8–11, two closed-loop simulations with different set-point profiles of $q$ and $\rho_{Te}^{*}$ are compared to a reference open-loop simulation with constant power levels in Figs. 12–15. The set-point profiles in the two closed-loop simulations are given as follows: the first closed-loop simulation (dashed curves in Figs. 12 and 15) has a monotonic $q$ and no ITB (small $\rho_{Te}^{*}$), and the second simulation (solid curves in Figs. 12 and 15) has a strongly reversed $q$ and a strong ITB (large $\rho_{Te}^{*}$). The actual set-point profiles are illustrated correspondingly in Figs. 13 and 14 by the dashed curves. The open-loop reference simulation with constant power levels is shown by the dotted curves (Figs. 12–15) and is the same simulation as shown already in Figs. 4–11.

As in all the simulations presented in section 3, the magnetic field, the plasma current, the plasma geometry, $Z_{eff}$, the initial and boundary conditions and the power levels of LHCD, NBI and ICRH, until the control starts, are taken from JET Pulse no: 62527. Again, to assess the controller effect on a fully developed steady state, the closed-loop simulations have been extended much further in time than the experiment itself that ended after $t$= 9.2s.

As one can see in Fig. 12 in the power levels of LHCD, NBI and ICRH, the three simulations start to deviate from each other immediately after $t$=5.5s when the real-time control starts. The predicted and the set-point $q$-profiles and $\rho_{Te}^{*}$-profiles for the same three simulations with the same colours at $t$=10s, $t$=20s and $t$=30s are illustrated in Figs. 13 and 15. The electron and ion temperature profiles at the same instants are shown in Figs. 15.

By having two extreme cases (difference between the dashed curves in Figs. 13 and 14) as the set-point profiles, the closed-loop simulations in Figs. 12–15 demonstrate that varieties of set-point $q$-profiles and $\rho_{Te}^{*}$-profiles are possible to achieve and control simultaneously. As found already with a single profile control in section 3, the time when the set-point values are reached may be of the order of the current diffusion time (~10–20s), i.e. longer than what can be experimentally achieved at high power on JET. Again, the reason for the long time to reach the set-point profiles in the simulations is that the initial $q$- and $\rho_{Te}^{*}$-profile were chosen quite far from the set-point profiles (extreme examples are shown here). As a consequence, smaller overall gains ($g_c$ and $g_c/\tau_i$) multiplying the controller has been used in the simulations, in order to guarantee the stability of the controller.

Within the limits of the present transport model, the simulation with the reversed $q$-profile and strong ITB as the set-point $\rho_{Te}^{*}$ -profile (solid curves in Fig. 14) also show the way to achieve strong ion ITBs, desirable for high fusion performance. The three different simulations presented

in Figs. 12–15 also demonstrate the fact that the variations due to the ITB appearance/disappearance in the $\rho_{\mathrm{Ti}}^{*}$-profiles are much larger than those in the $\rho_{\mathrm{Te}}^{*}$-profiles. This can be regarded as an indication that the real-time control of $\rho_{\mathrm{Ti}}^{*}$ could make sense and should be feasible, at least from the physics point of view.

Finally, the evolution of the 'squared distances', calculated as in equation (6), between the set-point and simulated profiles for the two closed-loop simulations (presented in Figs. 12–15) is shown in Fig. 16. Both the square distances–$dq^2$ (dashed) and $\mu^o d\rho_{\mathrm{Te}}^{*2}$ (dotted) of the $q$ and $\rho_{\mathrm{Te}}^{*}$ control, as well as the total square distance $dy^2$ (solid) are shown.

In the closed-loop simulation with the monotonic $q$ and no ITB as the set-point profiles (Fig. 16, top frame), the set-point profiles are reached well after $t$=10s and a steady-state solution on the controlled region is sustained until the end of the simulation. Before reaching the steady-state, the main contribution to the square distance comes from the difference between the simulated and set-point $q$-profile because the initial $q$ is reversed whereas the set-point $q$ is monotonic. In the closed-loop simulation with the reversed $q$ and strong ITB as the set-point profiles (Fig. 16, bottom frame), the set-point profiles are also reached rather well after $t$=10s. However, after $t$=20s the square distance from the $q$ control starts to gradually increase. This demonstrates that a steady-state solution is not found by the controller and indicates that the set-point $q$-profile is not and will not be a feasible solution with the set-point $\rho_{\mathrm{Te}}^{*}$-profile. The reason why $q$ deviates more strongly from the set-point value than $\rho_{\mathrm{Te}}^{*}$, i.e. $dq^2 > \mu^o d\rho_{\mathrm{Te}}^{*2}$, is that the value of $\mu^o$ was 70000 in the determination of the feedback controller. This choice seems to give too much weight on minimising the square distance of $\mu^o d\rho_{\mathrm{Te}}^{*2}$, at the expense of increasing the square distance of $dq^2$. The optimum value for $\mu^o$ seems to be somewhere between 10000 and 70000, depending on whether one wants to emphasise the $q$ or the $\rho_{\mathrm{Te}}^{*}$ control.

## 5. EXPERIMENTAL RESULTS WITH RTC AND A COMPARISON WITH THE SIMULATION RESULTS

A brief account of the recent RTC experiments performed on JET will now be given for completeness and for comparison with the simulations presented in section 4. Experimental details can be found in Refs. [7–10] and a summary of the results obtained with two different versions of the control algorithm a lumped-parameter and a distributed-parameter version of the controller is provided in Ref. [11].

For the second set of experiments which the present simulations refer to, the chosen reference scenario used a typical 1.7MA/3T reversed shear configuration obtained with 2.1MW of LHCD, 3MW of ICRH and 13.6MW of NBI, at a plasma electron density $n_{\mathrm{e}} \approx 3 \times 10^{19}\ \mathrm{m}^{-3}$. These powers were carefully selected in order to get an ITB while staying well below the operational limits in order to have enough headroom both in the open-loop power step experiments to identify the model and, later, in the closed-loop experiments. The Galerkin approximation of both the profiles on each set of basis functions (five coefficients for $i$ or $1/q$ and three for $\rho_{\mathrm{Te}}^{*}$) were computed in real-time from the profile measurements and, every 10ms, a proportional-integral power request was sent by

the controller to the different actuators. The control loop was applied for a maximum of 7 seconds and allowed different set-point $q$-profiles from monotonic to reversed shear ones to be reached successfully while simultaneously controlling the profile of the electron temperature gradient. Figure 17 shows the result in the case of a monotonic $q$-profile target, and of a $\rho_{\mathrm{Te}}^{*}$-profile target with a maximum slightly above the criterion for the existence of an ITB [18], at a fairly large radial location where ITB's are not easily achieved spontaneously. The effect of the controller is also shown in Fig.18 where the requested and achieved $q$, $i$ and $\rho_{\mathrm{Te}}^{*}$-profiles are represented at $t$=5.5s, 8s and 10.25s. Both profiles were satisfactorily controlled. In this pulse, the ICRH system technically failed to deliver the requested power at around $t$=10.3s, and therefore the control phase duration was limited to 4.8 seconds.

In different pulses (Pulse Nos: 62160 and 62527) a non-monotonic set-point $q$-profile was requested, together with a set-point $\rho_{\mathrm{Te}}^{*}$-profile with a maximum just above the ITB criterion. Such a reversed-shear $q$-profile target was chosen in order to test the controller further away from the reference state. The plasma current was almost fully non-inductively driven during the control time window. The effect of the controller is shown in Fig. 19 (pulse No: 62160, time traces) and also in Fig. 20 where the requested and achieved $q$, $i$ and $\rho_{\mathrm{Te}}^{*}$-profiles are represented for pulse no 62527 at $t$=6.95s, 8.4s and 9.15s.

Interestingly enough, both in Pulse No: 62156 ($t \approx 8.5$s) and No: 62160 ($t \approx 8$s), a sawtooth-like relaxation is observed on $\rho_{\mathrm{Te}}^{*}$ near $r/a$=0.6, and the controller nicely brings $\rho_{\mathrm{Te}}^{*}$ back towards its set-point value. Although the simulations do not exhibit such rapid phenomena where an ITB is lost, they are often observed experimentally in the ITB regime. Including these kinds of rapid phenomena, caused by for example MHD events, in the fully predictive closed-loop transport simulations with RTC is left for future work.

The accuracy of the controller to reach and sustain the set-point $q$- and $\rho_{\mathrm{Te}}^{*}$-profiles is roughly as good in the simulations as in the experiments. The biggest difference is the time when the set-point profiles are reached, the time being much longer in the simulations. However, in the simulations where the initial profiles of $q$ and $\rho_{\mathrm{Te}}^{*}$ are as close to the set-point profiles as typically in the experiments and thus larger constant and integral gains in the controller can be used in the simulations the time to reach the set-point profiles is similar. Another significant difference is the "purity" of the plasma between the simulations and experiments. The experiments tend to have all kinds of MHD activities, such as NTMs, ELMs, as well as varying $Z_{\mathrm{eff}}$ and plasma shape while the simulations are completely free from them. In addition, the experimental measurements suffer from diagnostics problems while in the simulations the values of the plasma profiles and the actuator power levels are known exactly. In that sense, the simulations serve as a simplified platform to test, validate and develop the real-time control algorithms and techniques, with increasing degrees of complexity and completeness.

## 6. CONCLUSIONS AND FUTURE PERSPECTIVES

A model-based multi-variable scheme has been implemented in the JETTO transport code as well as JET tokamak for the real-time control of distributed plasma parameters such as the current density, temperature, and/or pressure profiles. The proposed technique includes the identification of a distributed-parameter model with two different sets of appropriate basis functions for *q*-profile and $\rho_{Te}^*$, and using the Galerkin method for projecting the measured profiles onto the trial function bases. The electron temperature gradient control in the ITB was restricted to the plasma region where an ITB was expected (and requested) to emerge once a given set-point *q*-profile has been chosen. The technique amounts to the minimization of an integral square error signal which combines the two profiles, rather than attempting to control plasma parameters at some given radii with great precision. The resulting fuzziness of the control scheme allows the plasma to evolve towards a physically accessible non-linear state which may not be accurately known in advance, but is the closest to the requested one, and therefore provides the required plasma performance.

In the first phase of the simulations, the single profile, either the *q*-profile or the electron temperature gradient in the ITB ($\rho \neq_{Te}^*$), real-time control was performed with fully predictive JETTO transport simulations. Although the set-point profiles were achieved, and also sustained very nicely by the JETTO real-time controller, the controller in JETTO found some unexpected ways to minimise the integral square error signal (equation (6)). In the case of the reversed set-point *q*-profile (no $\rho \neq_{Te}^*$ control), the closed-loop simulation converged towards the set-point *q*-profile by turning off the NBI and ICRH powers and increasing the LHCD power above 6MW. On the other hand, in the case of the monotonic set-point *q*-profile (no $\rho_{Te}^*$ control), the closed-loop simulation first decreased all the three powers in order to get rid of the ITB and of the large off-axis bootstrap current due to the ITB. Otherwise the current density profile would not have peaked, thus preventing *q* from becoming gradually monotonic. In the closed-loop simulation with the 'strong ITB' as the set-point $\rho_{Te}^*$-profile (no *q* control), the simulation approached the requested $\rho_{Te}^*$-profile, but only in the electron heat transport channel. In fact, the ion temperature and the ion temperature gradient were the smallest in the simulation with the strong ITB as the set-point $\rho_{Te}^*$-profile. This was justified by the RTC controller because $\rho_{Te}^*$ measures and controls the electron temperature gradient, and electron temperature, rather than the ion ones. However, from the fusion performance point of view, the ITB on the ion heat transport channel is more desirable. This indicates that $\rho_{Ti}^*$ (ion Larmor radius divided by the ion temperature length) could be an equally or even more relevant quantity to be real-time controlled.

The closed-loop simulations of a single profile also demonstrated the existence of a double time scale in the case when controlling only the location and strength of the ITB ($\rho_{Te}^*$-profiles). Although the temperature profiles can be changed in principle on the energy confinement time scale, moving the ITB significantly outwards, i.e. changing the position of the peak in the $\rho_{Te}^*$-profile, took a much longer time. This was due to the fact that the location of the ITB (and the ITB dynamics in general) is strongly coupled with the *q*-profile and magnetic shear evolution. As a consequence,

moving the footpoint of the ITB outwards may actually take a time of the order of the resistive current diffusion time, to allow significant changes in the *q*-profile to occur. This phenomenon demonstrated well the coupling of the two different time scales the fast energy confinement time and the slow resistive current diffusion time both governing the control of the electron temperature and electron temperature gradient in the ITB ($\rho\neq_{Te}^{*}$ control). These simulations therefore support the design of a double time scale real-time controller for a successful ITB control in discharges whose duration is of the order of the resistive current diffusion time.

As the second, more advanced step, the real-time control of two plasma profiles simultaneously were performed with JETTO transport simulations. The simulations were carried out in a plasma regime with an internal transport barrier to control the strength and location of the ITB by applying RTC simultaneously to the current density or the *q*-profile and the electron temperature gradient profile ($\rho\neq_{Te}^{*}$ control). The simulations with the combined real-time control demonstrated that varieties of set-point *q*-profiles and $\rho_{Te}^{*}$-profiles are possible to achieve and control simultaneously. And very importantly, the successful control could be continued for several resistive current diffusion times. Therefore, within the limits of the present transport model, the simulation with the reversed *q*-profile and strong ITB as the set-point $\rho\neq_{Te}^{*}$-profiles showed a way to achieve strong ion ITBs in a controllable way, desirable and necessary for high fusion performance in long pulse experiments.

These simulations also supported strongly the experimental results that the real-time control of *q* and $\rho_{Te}^{*}$-profiles can be carried by using the real-time control techniques presented in Refs. [7-9]. Although no transport model/simulation can predict the experiments perfectly, they are very useful in developing and testing more complex RTC algorithms, before implementing these into the experimental control systems. As transport models do not reproduce the experimental results identically, the static linear response
$K(0)$ of the controller used in the simulations is different from that in the experiments. This is due to the response from the open-loop power step-up simulations being not identical to that from the open-loop power step-up experiments. On the other hand, transport simulations are free from unpredictable events, such as MHD events, diagnostics problems or power systems failures occurring often in the experiments. Therefore, the simulations serve as a simplified platform to test, validate and develop the real-time control algorithms techniques (described below), with increasing degrees of complexity and completeness.

Improved model identification methods are now under development. The identification (both experimental and simulated) of a fully dynamic linear model $K(s)$ is now under investigation in preparation of the 2005-2006 JET experimental campaign. This dynamic response will be used to try and construct a two-timescale model and design a controller which may respond faster to rapid plasma events such as the emergence, collapse and displacement of the ITB (occurring on a confinement time scale), while converging slowly towards the requested high performance plasma state (resistive time scale). The closed-loop RTC simulations showed that present approximation using the static linear response $K(0)$ is good enough when the rapid plasma events are absent.

However, the dynamical response $K(s)$ is probably needed when the rapid plasma events are included in the simulations. Future plans also include the integration of the ion temperature and plasma density in the controlled profiles, as well as the extension of the actuators, such as gas injection. Numerical, fully predictive transport modelling provides a very useful qualitative assessment of the control algorithms and will be used for the preparation of ITER scenarios.

**REFERENCES**


[1]. T.S. Taylor 1997 *Plasma. Phys. Control. Fusion* **39** B47.

[2]. J. Connor *et al*. 2004 *Nucl. Fusion* **44** R1.

[3]. C. Challis "The use of internal transport barriers in tokamak plasmas" 2004, to be published in"*Plasma. Phys. Control. Fusion*.

[4]. T.J.J. Tala *et al*. 2001 *Plasma. Phys. Control. Fusion* **43** 507.

[5]. E. Joffrin *et al*. 2002 *Plasma. Phys. Control. Fusion* **44** 1739.

[6]. X. Garbet *et al*. 2003 *Nucl. Fusion* **43** 975.

[7]. D. Moreau *et al*. 2003 *Nucl. Fusion* **43** 870.

[8]. D. Mazon *et al*. 2003 *Plasma. Phys. Control. Fusion* **45** L47.

[9]. L. Laborde *et al*. "A model-based technique for integrated real-time profile control in the JET tokamak", 2004 accepted for publication in *Plasma Phys. Control. Fusion*.

[10]. D. Mazon *et al*., 31st EPS Conference, London, 2004, ECA Vol **28G**, P5.168.

[11]. D. Moreau *et al.*, "Development of Integrated Real-Time Control of Internal Transport Barriers in Advanced Operation Scenarios on JET", IAEA Fusion Energy Conference, Vilamoura, Portugal, 2004, Paper EX/P2-5.

[12]. G. Genacchi and A. Taroni "JETTO: a Free Boundary Plasma Transport Code (Basic Version), Rep. ENEA RT/TIB 1988(5), ENEA (1988).

[13]. T.J.J. Tala *et al*. (2004) "Fully Predictive Transport Simulations of ITB Plasmas in JET, JT-60U and DIII-D", IAEA Fusion Energy Conference, Vilamoura, Portugal, 2004, Paper TH/P2-9.

[14]. T.J.J. Tala *et al*. (2004) "Fully Predictive Transport Simulations of ITB Plasmas in JET, JT-60U and DIII-D", submitted to *Nucl. Fusion.*

[15]. M. Erba *et al*. 1997 *Plasma. Phys. Control. Fusion* **39** 261.

[16]. J. Weiland, ''Collective Modes in Inhomogeneous Plasma'', Institute of Physics Publishing, Bristol, (2000).

[17]. W. Houlberg et al. (1997) Phys. Plasmas **4** 3231.

[18]. G. Tresset, et al., 2002 Nucl. Fusion **42** 520.

[19]. A.R. Esterkin and A.D. Piliya 1996 *Nucl. Fusion* **36** 1231.

[20]. C.D. Challis et al. 1989 *Nucl. Fusion* **29** 563.

[21]. L.G. Eriksson, T. Hellsten, U. Willen 1993 *Nucl. Fusion* **33** 1037.

[22]. L. Lao et al. 1985 *Nucl. Fusion* **25** 1611.

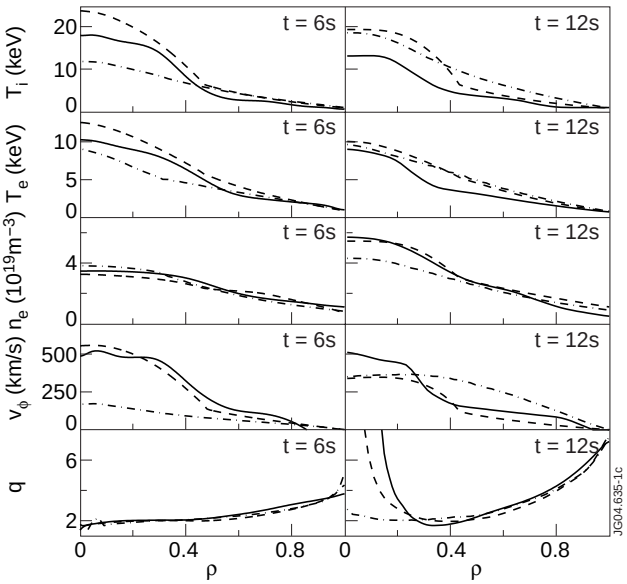


*Figure 1: Model predictions for the 5 predicted plasma profiles compared with the experiments for JET Pulse No: 46664 t=6.0s (left) and 53521 at t=12.0s (right). The solid curves correspond to the experimental value and the dashed and dash-dotted curves to the predictions by the Bohm/GyroBohm and Weiland transport models, respectively.*

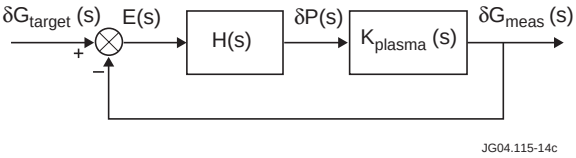


*Figure 2: $\acute{G}_{target}$ and $\acute{G}_{meas}$ denotes the set of Galerkin coefficients for the difference between the set-point and simulated profiles, E is the error signal and $\acute{P}$ the power request by the controller.*

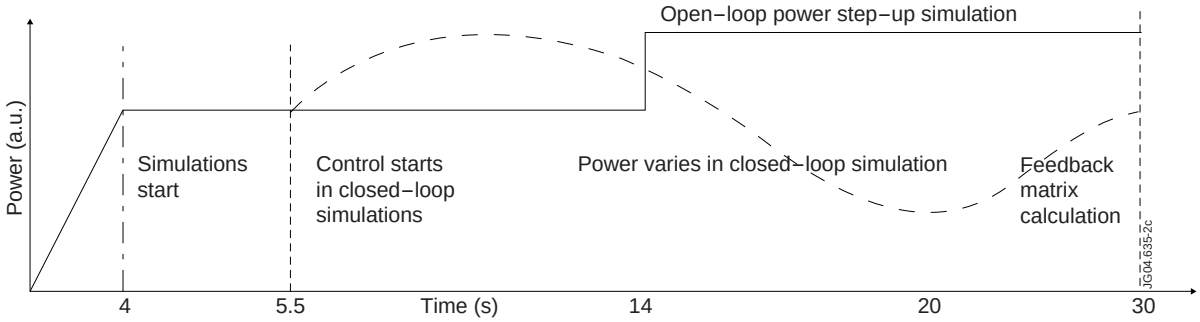


*Figure 3: A schematic view on how to perform open- and closed-loop transport simulations with JETTO. Times refer to typical times in JET ITB discharges and used in the predictive simulations.*

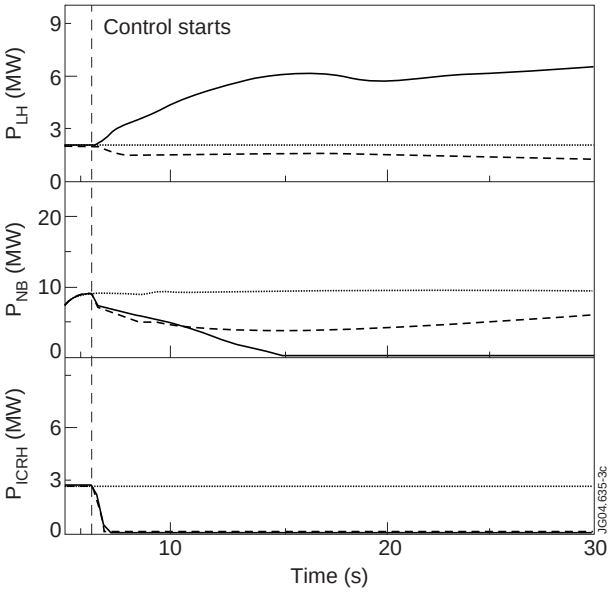


*Figure 4: Power levels of two closed-loop simulations, one with a reversed set-point q-profile (solid) and one with a monotonic set-point q-profile (dashed). Also shown a reference open-loop simulation (dotted) with constant power levels of LHCD, NBI and ICRH. The control starts at t=5.5s.*

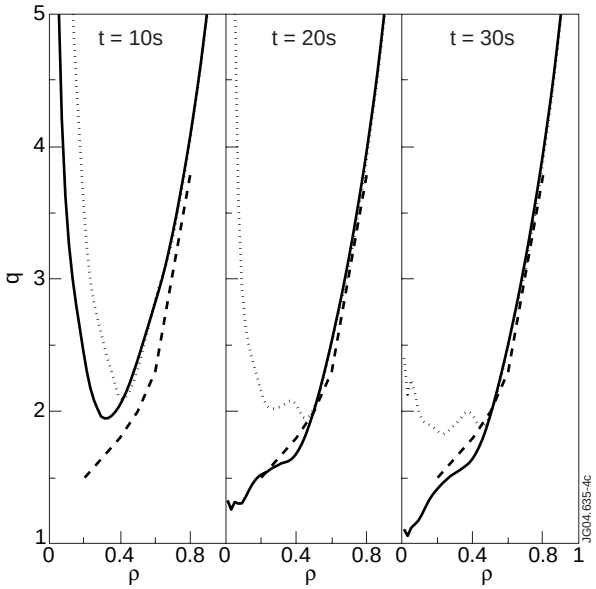


*Figure 5: q-profiles for the closed-loop simulation with a monotonic set-point q-profile (solid) and the reference open-loop simulation (dotted) at t=10s, t=20s and t=30s.The dashed curve is the set-point q-profile used in the closed-loop simulation.*

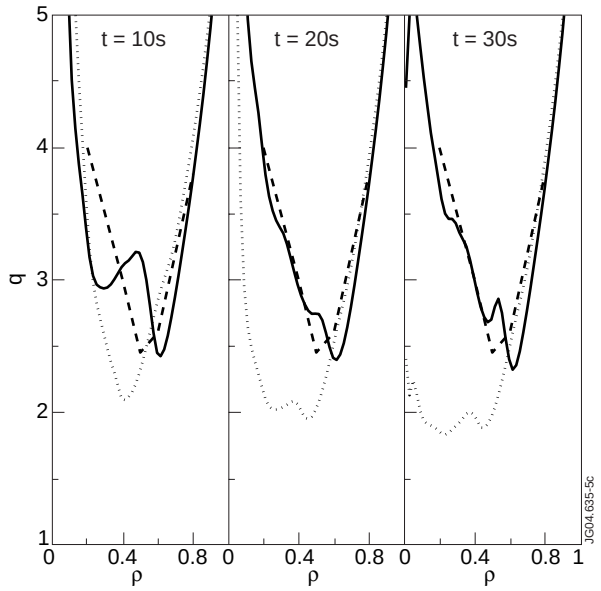


*Figure 6: As in Fig. 5, but for the q-profiles for the closed-loop simulation with the reversed set-point q-profile (solid) and a reference open-loop simulation (dotted) at t=10s, t=20s and t=30s.The dashed curve is the set-point q-profile used in the closed-loop simulation.*

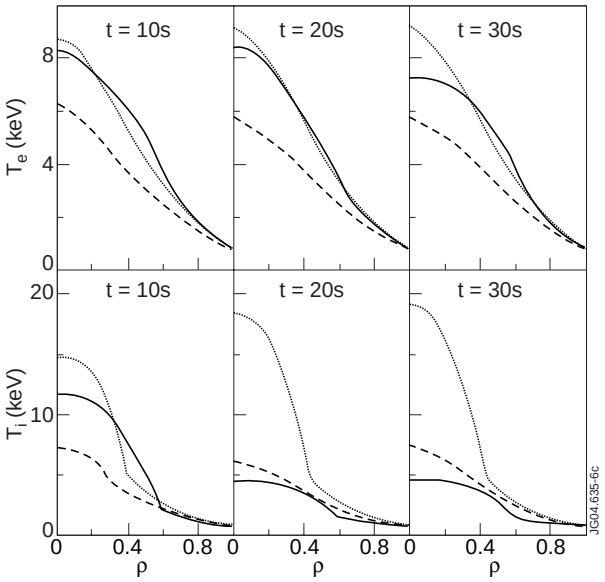


*Figure 7: The electron and ion temperature profiles for the two closed-loop simulations and the open-loop reference simulation. The solid and dashed curves correspond to the closed-loop simulations with reversed and monotonic set-point q-profiles, respectively, and the dotted curves to the open-loop simulation.*

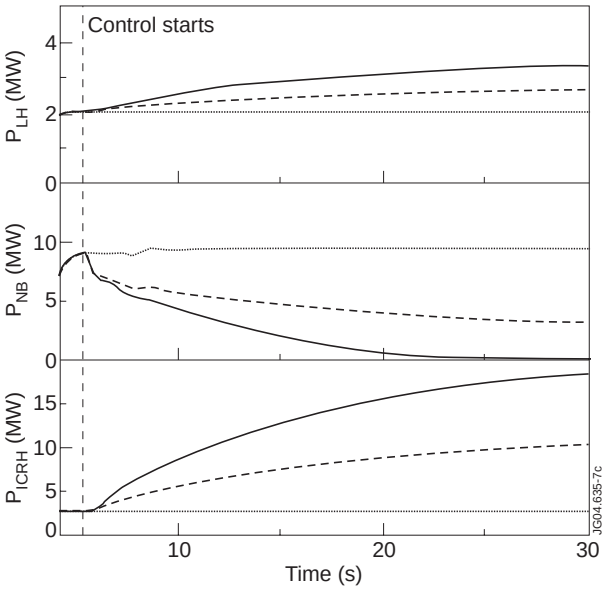


*Figure 8: Power levels of two closed-loop simulations, one with a 'strong ITB' set-point $\rho_{Te}^*$-profile (solid) and one with a 'weak ITB' set-point $\rho_{Te}^*$-profile (dashed). Also shown the reference open-loop simulation (dotted) with constant power levels of LHCD, NBI and ICRH. The control starts at t=5.5s.*

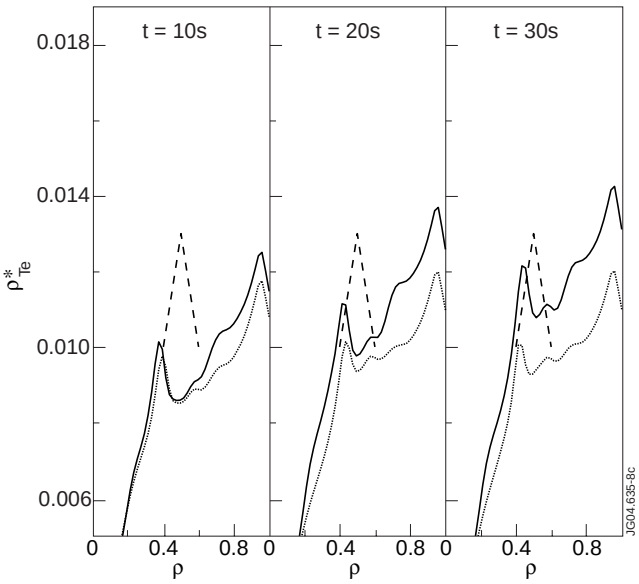


*Figure 9: $\rho_{Te}^*$-profiles for the closed-loop simulation with a'weak ITB' set-point $\rho_{Te}^*$-profile (solid) and the reference open-loop simulation (dotted) at t=10s, t=20s and t=30s. The dashed curve is the set-point $\rho_{Te}^*$-profile used in the closed-loop simulation.*

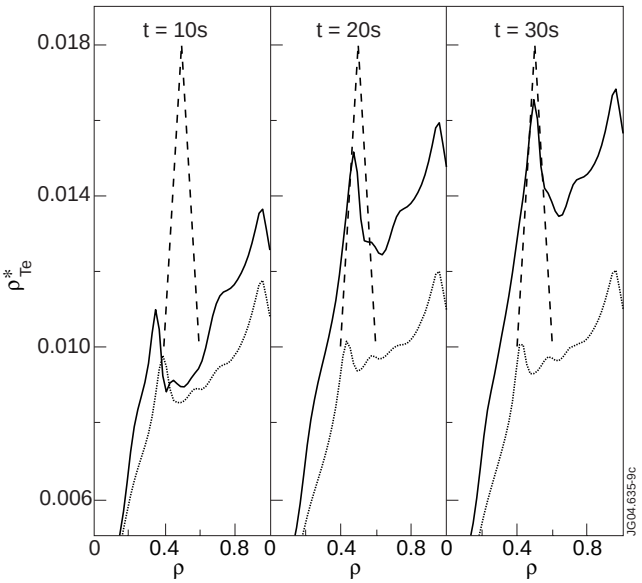


*Figure 10: As in Fig. 9, but for the $\rho_{Te}^*$-profiles for the closed-loop simulation with a'strong ITB' set-point $\rho_{Te}^*$-profile (solid) and the reference open-loop simulation (dotted) at t=10s, t=20s and t=30s. The dashed curve is the set-point $\rho_{Te}^*$-profile used in the closed-loop simulation.*

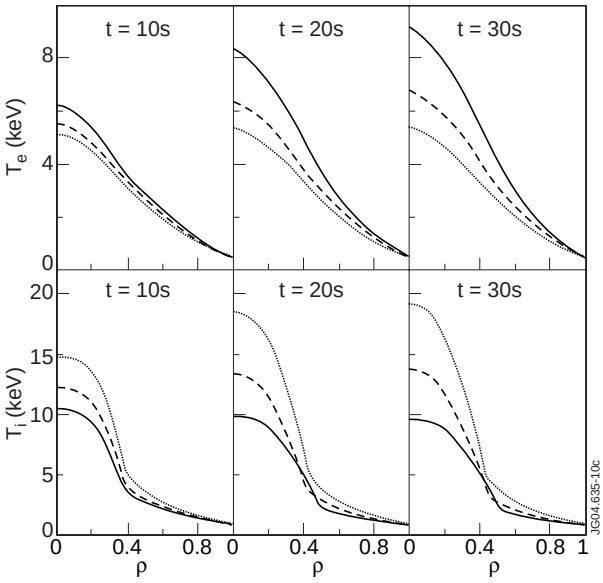


*Figure 11: The electron and ion temperature profiles for the two closed-loop simulations and the open-loop reference simulation. The solid and dashed curves correspond to the closed-loop simulations with a strong and weak ITB set-point $\rho_{Te}^*$-profiles, respectively, and the dotted curves to the open-loop simulation.*

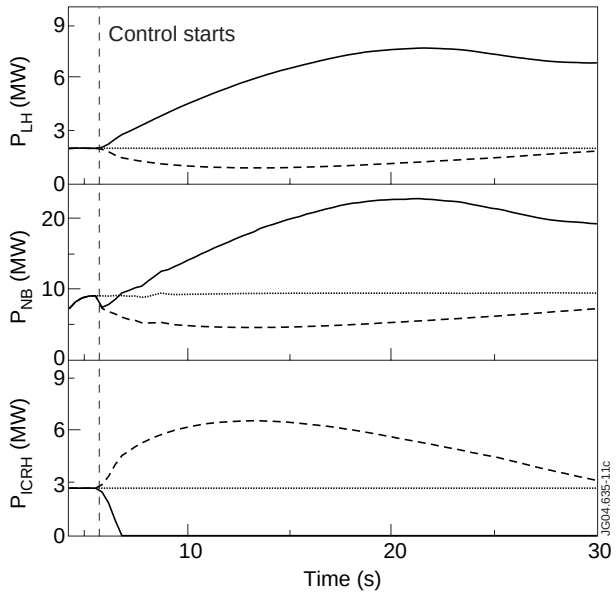


*Figure 12: Power levels of two closed-loop simulations, one with a monotonic set-point q-profile and no ITB set-point $\rho_{Te}^*$-profile (dashed) and one with a reversed set-point q-profile and a strong ITB set-point $\rho_{Te}^*$-profile (solid). Also shown the reference open-loop simulation (dotted) with constant power levels of LHCD, NBI and ICRH. The control starts at t=5.5s.*

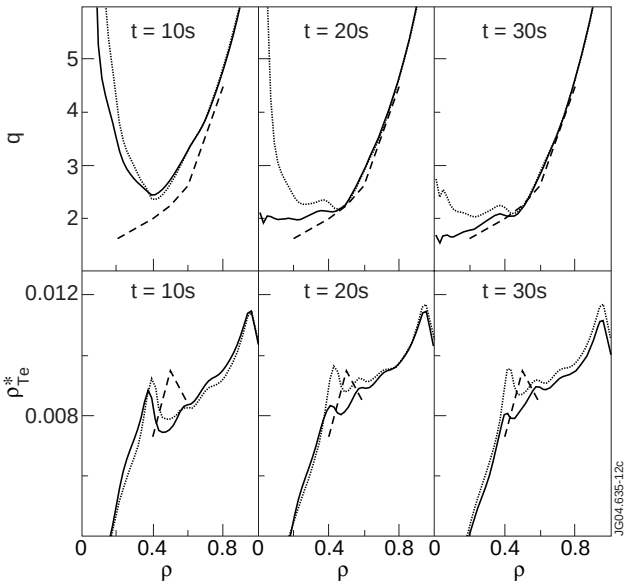


*Figure 13: q-profiles and $\rho_{Te}^*$-profiles for the closed-loop simulation with a monotonic set-point q-profile and no ITB set-point $\rho_{Te}^*$-profile (solid curves) at t=10s, t=20s and t=30s. The set-point q-profile and $\rho_{Te}^*$-profile are shown by the dashed curves and the reference open-loop simulation by the dotted curves.*

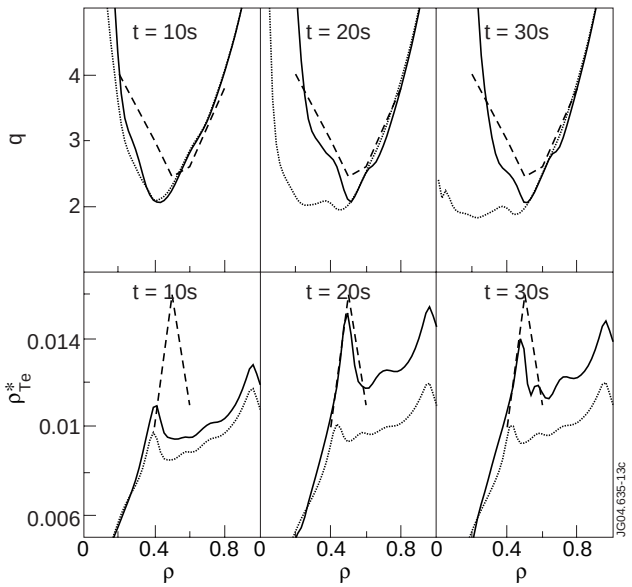


*Figure 14: As in figure 13, but for the closed-loop simulation with a reversed set-point q-profile and strong ITB set-point $\rho_{Te}^*$-profile (solid curves). The set-point q-profile and $\rho_{Te}^*$-profile are shown by the dashed curves and the reference open-loop simulation by the dotted curves.*

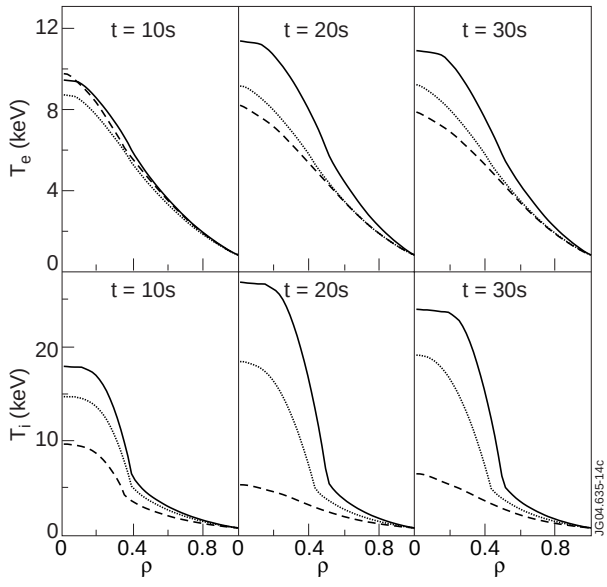


*Figure 15: The electron and ion temperature profiles for the two closed-loop simulations and the open-loop reference simulation. The solid and dashed curves correspond to the closed-loop simulations with a reversed set-point q-profile and a strong ITB set-point $\rho_{Te}^*$-profile (solid), and a monotonic set-point q-profile and no ITB set-point $\rho_{Te}^*$-profile (dashed). The dotted curves are from the open-loop simulation.*

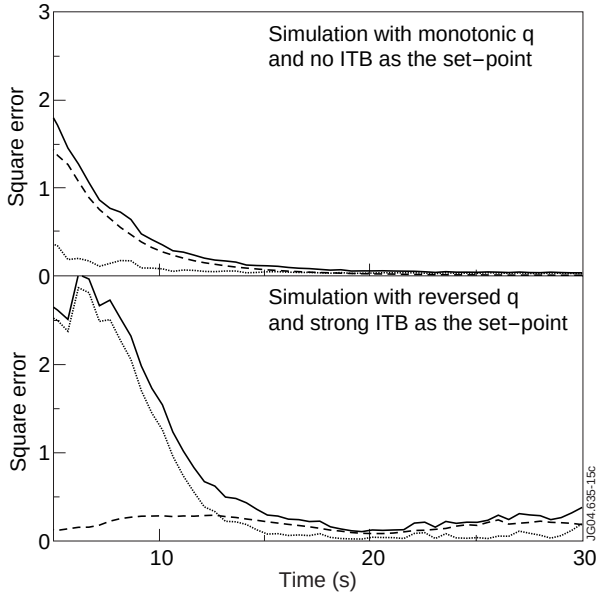


*Figure16: The total squar e distances (solid) between the simulated and set-point q-profiles and $\rho_{Te}^{*}$ -profiles as a function of time for the simulation with the monotonic q and no ITB (top) and with the reversed q and strong ITB (bottom) as the set-points. The square distances $dq^2$ (dashed) and $\mu^o d\rho_{Te}^{*2}$ (dotted) as well as the total square distance $dy^2$ (solid) are shown.*

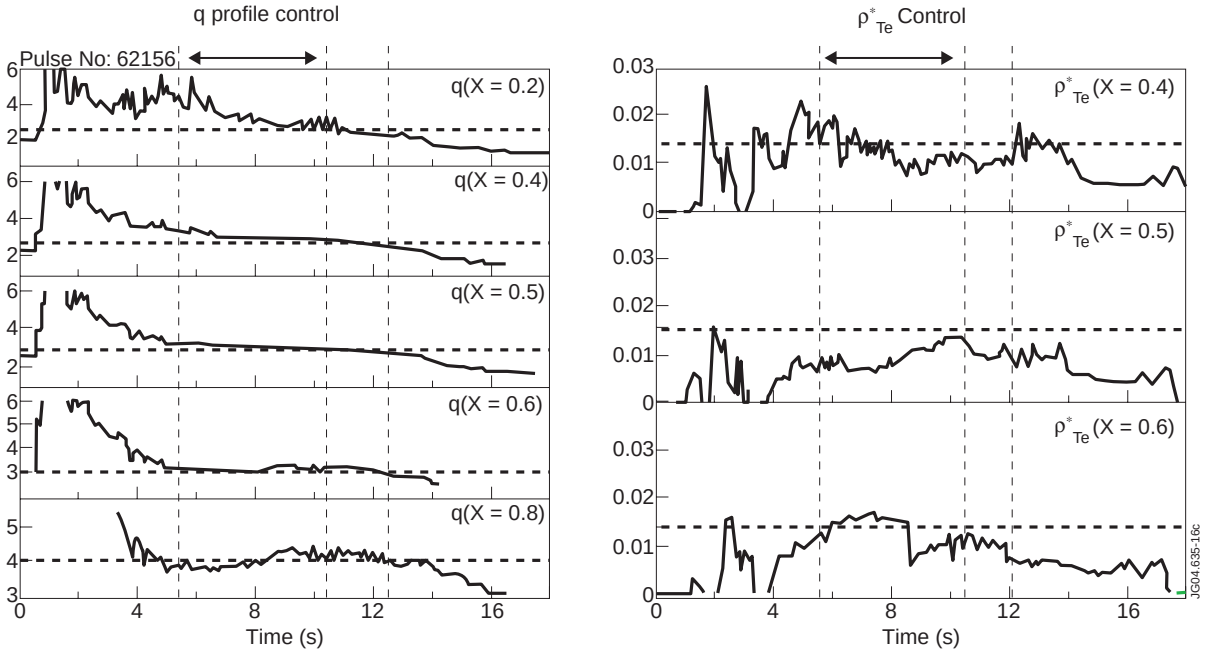


*Figure 17: Time evolution of the measured (solid curves) and requested (dashed lines) q values at 5 radii (left), and $\rho_{Te}$* values at 3 radii (right) for a controlled pulse having a monotonic set-point q-profile (pulse No :62156 $B_T$=3T $I_p$=1.7MA). The current flat top starts at 4s. Control starts at 5.5s until 12.3s (vertical dashed lines), but the ICRH power trips at 10.3s, as shown by the middle dashed line.*

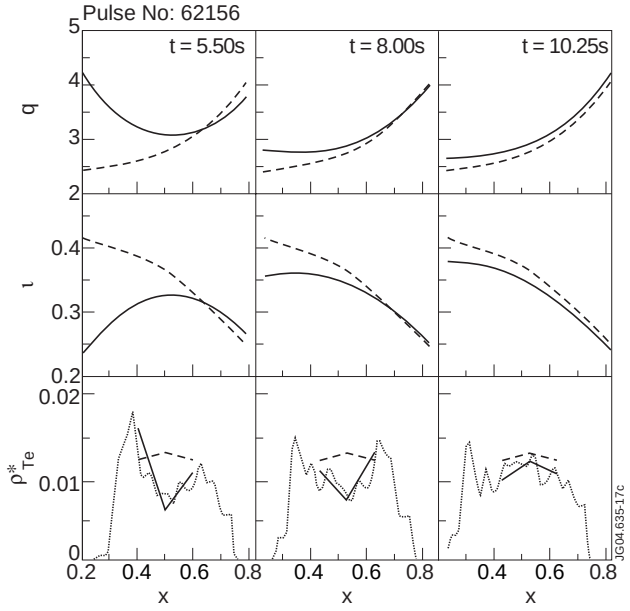


*Figure 18: Measured (solid) and set-point profiles (dashed) for q, $\pi$ and $\rho_{Te}^{*}$ after projection on the basis functions, for Pulse No: 62156 ($B_T$=3T , $I_P$=1.7MA, $n_e$=3×10$^{19}$m$^{-3}$). For $\rho_{Te}^{*}$, the original profile is also shown (dotted).*

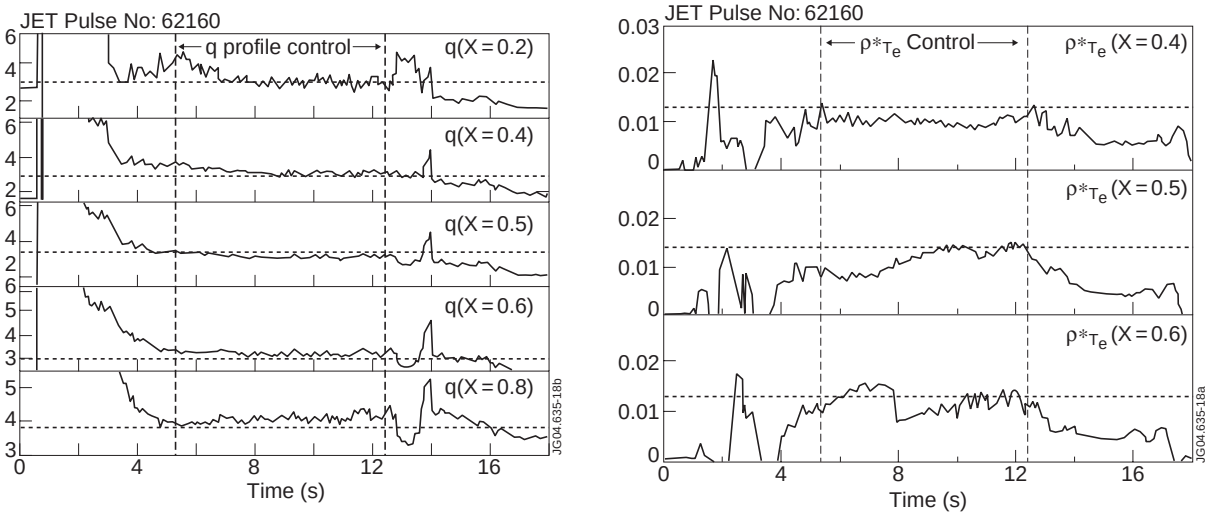


*Figure 19: Time evolution of the measured (solid curves) and requested (dashed lines) q values at 5 radii (left) and $\rho_{Te}^{*}$ values at 3 radii (right) for a reversed-shear controlled pulse (Pulse No: 62160, $B_T$=3T, $I_p$=1.7MA, $n_e$=3×10$^{19}$m$^{-3}$). The current flat top starts at 4s. Control starts at 5.5s and stops at 12.3s, as indicated by the vertical dashed lines.*

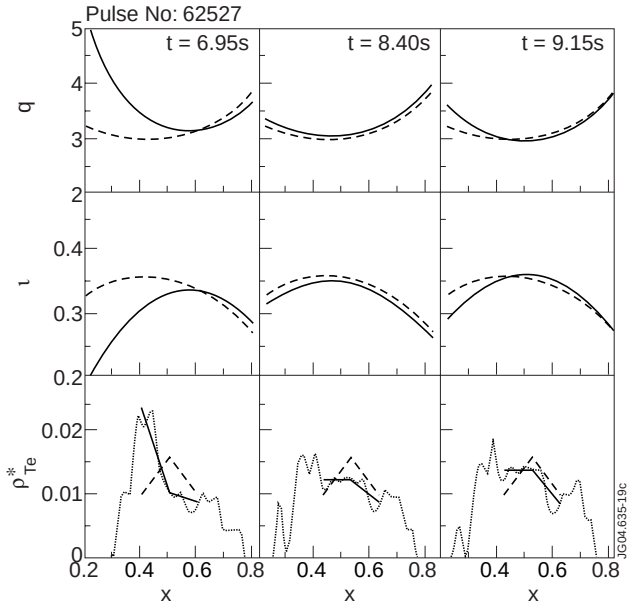


*Figure 20: Measured (solid) and set-point profiles (dashed) for q, $\pi$ and $\rho_{Te}^{*}$ after projection on the basis functions, for Pulse No: 62527 ($B_T$=3T , $I_P$=1.7MA, $n_e$=3.5×10$^{19}$m$^{-3}$). For $\rho_{Te}^{*}$, the original profile has also been plotted (dotted).*